CLOUDS AND INSTABILITIES IN SUPERNOVA REMNANT STRUCTURE: INTERSTELLAR TURBULENCE AND RIPPLED SHOCKS

J. C. Raymond

Harvard-Smithsonian Center for Astrophysics, USA

RESUMEN

Las hermosas ondas de choque esféricas de la teoría se desbaratan por la interacción con inhomogeneidades de densidad y por las inestabilidades térmicas y dinámicas. A través de varios trucos, involucrando las velocidades de corrimiento Doppler o suposiciones de los modelos, se puede construir una idea tridimensional de la estructura a partir de una imagen bidimensional. En este artículo discutiremos la naturaleza esperada de las inhomogeneidades de densidad y las consecuencias para la apariencia de un remanente de supernova, junto con las condiciones necesarias para algunas inestabilidades, y se presentará un ejemplo de los intentos de desenredar el problema y se discutirá el papel de la turbulencia interestelar.

ABSTRACT

The beautiful spherical blastwaves of theory are disrupted by interaction with density inhomogeneities and by thermal and dynamical instabilities. Various tricks, involving either Doppler shift velocities or model assumptions, make it possible to construct a 3-D picture of the structure from a 2-D image. This paper will discuss the expected nature of the density inhomogeneities and the consequences for the appearance of an SNR, along with the conditions for some instabilities, and it will present an example of attempts to sort it all out and discuss the role of interstellar turbulence.

Key Words: **SHOCK WAVES — SUPERNOVA REMNANTS — TURBULENCE**

1. INTRODUCTION

To first order, supernova remnants (SNR) are spherical, but real SNRs show significant deviations from spherical shape. Large deviations come about when the SNR blast wave hits a dense cloud (Levenson, Graham, & Walters 2003). The large deviation implies a large density contrast, and the resulting shock in the cloud is usually a radiative one, in which the shocked gas cools and most of the energy dissipated by the shock is converted to radiation. Large deviations can also occur if the blast wave encounters a large low-density region, resulting in a blowout. Either sort of large deviation can drastically affect the evolution of the remnant.

In some cases another sort of deviation is seen. The optical filaments of SN 1006 and the faint filaments that enclose the northern Cygnus Loop show small amplitude undulations, epitomizing the interpretation of SNR filaments as tangencies between a gently rippled sheet of emitting gas and the line of sight (Hester 1987). Beautiful examples can be seen in the Hα images of SN 1006 (Winkler & Long 1997) and the Cygnus Loop (Hester, Danielson, &

Raymond 1986; Ghavamian et al. 2001). The *HST* image of one filament is the most spectacular example (Blair et al. 1999), showing that the sheet emitting Hα is less than 10^{15} cm thick and very smooth. Levenson et al. (1998) show how the Hα filaments around the northern Cygnus Loop bound the X-ray emission. Figure 1 shows an example from the northern Cygnus Loop. This Hα image is centered on the position studied at optical wavelengths by Ghavamian et al. (2001) and in the UV and X-ray by Raymond et al. (2003). We will analyze this region in more detail below.

The smoothly rippled surfaces have in common that they are pure Balmer line filaments, which are interpreted as non-radiative shocks (Chevalier & Raymond 1978). The Balmer line emission arises when neutral hydrogen atoms swept up by the shock are excited before they are ionized. The emission is rather faint, because the average atom emits only about 0.2 photons, but the forbidden lines that dominate the optical spectra of radiative interstellar shocks are far fainter. Several permitted lines in the ultraviolet are reasonably bright, however, and
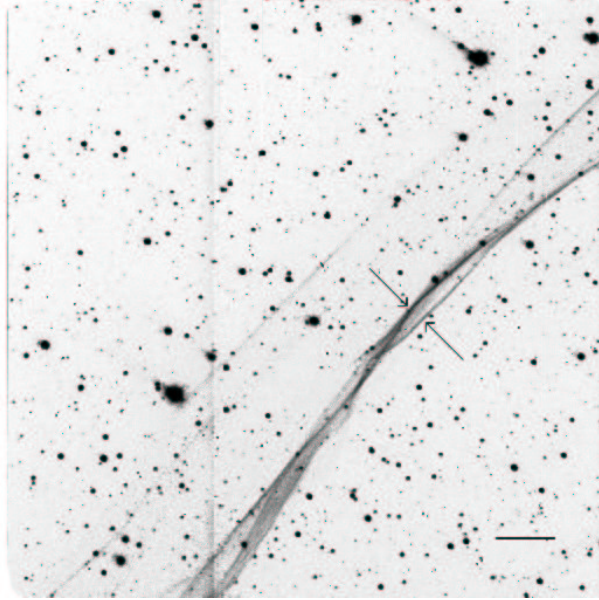
Fig. 1. Hα image of the non-radiative shock. Four *FUSE* spectra separated by about 5″ were obtained with the 20″ by 4″ slit parallel to the filaments between the two arrows. The image is 11′ on a side, and the bar in the lower-right corner indicates 1′.

they have been exploited to explore the physics of collisionless shock waves. The profiles of the Balmer lines and the UV lines provide powerful diagnostics for the thermal equilibration of electrons and ions in the gas just behind the shock (Long et al. 1992; Hester et al. 1994; Raymond, Blair, & Long 1995; Laming et al. 1996; Ghavamian et al. 2001, 2002).

One possible explanation for the ripples is an instability in the shock. The thermal instability, or more precisely overstability, has been extensively investigated, both analytically (Bertschinger 1986) and numerically (Gaetz, Edgar, & Chevalier 1988; Innes, Giddings, & Falle 1987; Innes 1992). Thermal instability is undoubtably responsible for much of the complex structure of radiative shocks as compared with non-radiative ones. It results from the high radiative cooling rate at temperatures above 10^5 K, and it is catastrophic for shock speeds above about $150 \, \mathrm{km \, s^{-1}}$ where the sound crossing time exceeds the cooling time. The transverse scale of the resulting structures should be comparable to the cooling length. Another possibility is the thin shell instability (Vishniac 1983). Again, this is actually an overstability. It depends upon the misalignment of the ram pressure of the shock with the thermal pressure that drives it when the shock is rippled. The thin shell instability requires a compression ratio above 10, or $\gamma < 1.2$ for a shock in a perfect gas

(Vishniac & Ryu 1989). Neither the thermal instability nor the thin shell instability is consistent with a non-radiative shock.

It is also possible that the deformation of the shock reflects inhomogeneity of the hot gas driving it. This could result from shrapnel of the original explosion or from Rayleigh-Taylor fingers generated at the contact discontinuity between shocked intestellar medium (ISM) and shocked ejecta during the transtion to the Sedov phase (e.g., Wang & Chevalier 2001). This would seem plausible for SN 1006, and indeed *Chandra* observations show enriched ejecta gas within a few arcseconds of the shock front (Long et al. 2003). It seems very unlikely that the blast wave of a remnant as old as the Cygnus Loop would be affected by clumps of ejecta. However, the apparently ejecta-driven bowshocks at the periphery of the Vela Supernova Remnant (Aschenbach, Egger, & Trümper 1995) show that this possibility must be considered. Nevertheless, even with the smaller distance to the Cygnus Loop of 440 pc (Blair et al. 1999), the swept-up mass of the Cygnus Loop is quite large, and no obvious ejecta bowshocks are seen.

If none of these mechanisms can account for the rippled appearance of non-radiative shocks, the obvious remaining explanation is small amplitude density variation in the pre-shock gas. Fluctuations ought to be present at some level, as studies of interstellar turbulence apparently show a Kolmogorov spectrum of many orders of magnitude (e.g., Minter & Spangler 1996), though Cho, Lazarian, & Vishniac (2002) have recently shown that magnetic and density fluctuations behave differently below the viscous scale of order 0.1 pc.

A non-radiative shock in the northern Cygnus Loop was studied extensively by Ghavamian et al. (2001) and Raymond et al. (2003). Here we consider the implications for small-amplitude density fluctuations in the pre-shock medium.

2. CYGNUS P7

A continuous arc of faint optical filaments bounds the northern Cygnus Loop, generally showing a pure Balmer line emission spectrum. Filaments in the northwest were analyzed by Raymond et al. (1980) and Treffers (1981). Those in the northeast were studied by Raymond et al. (1983), Fesen & Itoh (1985), Hester et al. (1994), Long et al. (1992), Blair et al. (1999), Sankrit et al. (2000), and Sankrit & Blair (2002). Interpretation of the NE filaments was somewhat ambiguous, because the filaments studied there are making the transition from non-radiative to radiative shocks.

A filament in the northern Cygnus Loop was chosen for study with the *Hopkins Ultraviolet Telescope*, ground-based telescopes, and *FUSE* based on its lack of any signatures of cooling and its probable higher shock speed. For lack of a better name, it is known by its designation for the *HUT* observing program as Cygnus P7. It is located at the center of Fig. 1, an Hα image obtained at the FLWO 1.2 m telescope (Raymond et al. 2003). Images in [O III] show no emission near the region studied. Images in [Ne V] using the set-up described by Szentgyorgyi et al. (2000) show no detectable emission.

Ghavamian et al. (2001) obtained Hα and Hβ profiles with the FAST spectrograph on the 1.6 m telescope at FLWO. Analysis of the profiles included Monte Carlo radiative transfer calculations for the Lyβ and Lyγ lines, along with grids of models with different shock speeds and degrees of electron-ion equilibration at the front. Comparison of the models with the observed profiles implies $T_e/T_i > 0.7$ at the shock front and a shock speed $V_s = 300$ to $365\,\mathrm{km\,s^{-1}}$.

Raymond et al. (2003) observed the same position with the *Hopkins Ultraviolet Telescope*. The absence of any emission other than the O VI, C IV and He II lines confirms the non-radiative character of the shock. The line profiles show that the kinetic temperature of oxygen is less than 2.7 times the kinetic temperature of the protons, confirming the conclusion of Ghavamian et al. (2001) that thermal equilibration is efficient in this relatively slow shock. Raymond et al. (2003) also determined the *ROSAT* PSPC count rate as a function of distance behind the shock. The *ROSAT* data constrain the shock speed to the upper end of the range allowed by the optical line profiles, and we adopt $V_s = 350\,\mathrm{km\,s^{-1}}$.

FUSE spectra were obtained with the MDRS slit parallel to the shock at the main shock front and at three positions spaced back from it by about $6''$, $11''$, and $15''$. The O VI $\lambda 1032$ profiles are shown in Figure 2.

The double-peaked profiles imply either absorption at line center or a line of sight that passes through the rippled shock in two places, one approaching the Sun and one receding. To sort out the nature of the profiles, we constructed models of the emitting sheet including the effects of resonance scattering.

3. MODELS

Models of the ionization structure behind nonradiative shocks indicate an optical depth normal to the shock of order 0.1 in the O VI $\lambda 1032$ line.
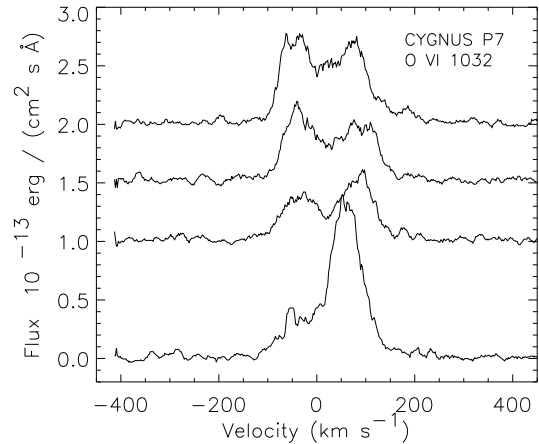

Fig. 2. Profiles of the O VI $\lambda 1032$ line at the bright filament (top profile) and the 3 offset positions behind it.

The edge-on viewing geometry of the filament implies optical depths along the line of sight of order one. Therefore, the effects of scattering must be included. We computed plane-parallel shock models with a current version of the code described by Raymond (1979) for various choices of model parameters, in particular the pre-shock density. The predicted ionization state and emissivity were then used to specify the emission and absorption in a two-dimensional grid for a chosen shape of the shock ripple. The existence of two parallel filaments implies two tangencies to the line of sight, Figure 3 shows one such shape. Note that the x-scale is compressed by a factor of 5 compared with the y-scale, so the ripple is in fact quite gentle. The excursion to large y is in keeping with the existence of faint Hα and X-ray emission ahead of the main filament due to material ahead of the shock as seen in projection.

The numerical code simply computes the intensity along any given line of sight in $10\,\mathrm{km\,s^{-1}}$ bins. The shock shape and preshock density are then adjusted to match the observed line profiles. Within the constraints from other observations, variation in shock speed, magnetic field, and electron-ion equilibration are unimportant. Further constraints are provided by the *ROSAT* X-ray emission. In essence, both the line profiles and the X-ray surface brightness are used to compare quantities proportional to $n_e^2 L$ (X-ray brightness, O VI emissivity) with one proportional to $n_e L$ (optical depth) in order to disentangle n_e from the line-of-sight depth, L. Further constraints arise from the fact that the splitting of the peaks of the O VI profile increases with the curvature of the shock front, and therefore with $1/L$.
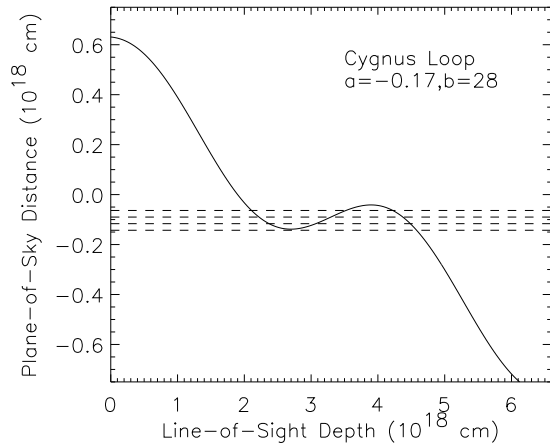
Fig. 3. Shape of the emitting filament derived by matching the observed O VI line profiles. Note that the vertical scale is expanded by about a factor of 5. Dashed lines indicate the lines of sight of the four exposures.

The *ROSAT* data provide constraints both from the dependence of the thickness of the initial ionization zone on density and the absolute brightness. Similar techniques for sorting out the 3-D structure of Cygnus Loop shocks have been employed by Raymond et al. (1988), Szentgyorgyi et al. (2000), and Patnaude et al. (2002).

The overall result is that the pre-shock density is between 0.3 and $0.5\,\mathrm{cm}^{-3}$, about twice the canonical value based on global X-ray models. Global models for the X-ray emission based on a $440\,\mathrm{pc}$ distance would probably yield densities in agreement with the higher value. The optical depth in the O VI $\lambda1032$ line is about one near line center just behind the bright filament, and somewhat smaller behind it. The depth of the emitting region along the line of sight is 0.7 to $1.5\,\mathrm{pc}$.

4. ISM DENSITY FLUCTUATIONS

As discussed in the Introduction, hydrodynamic instabilities are unlikely to account for the rippled shape of the shock. Therefore, the ripples probably arise from small-amplitude variations in the density, which translate into velocity variations. An accurate assessment of the density fluctuations should be made by propagating shocks through randomly selected realizations of Kolmogorov (or other) spectra of density variations. A crude estimate can be made by assuming that the amplitude of the ripple, about 0.1 of the wavelength, is equal to $\delta V/V$. For constant ram pressure, $\delta n_0/n_0 \sim 0.2$ at scales comparable to the wavelength of the ripples. Thus $\delta n_0 \sim 0.08\,\mathrm{cm}^{-3}$

at scales of order 10^{18} cm. For comparison, the typical variance in electron density derived from radio scintillation studies is $\langle \delta n_{\mathrm{e}} \rangle = 0.016\,\mathrm{cm}^{-3}$ at a scale of 10^{18} cm (S. Spangler 2002, private communication). Considering that the pre-shock gas is roughly half ionized and that the filling factor of the warm neutral medium is less than one half, this agreement is so good that it must be fortuitous. Nevertheless, it does suggest that a systematic measurement of the wavelengths and scales of ripples in non-radiative shocks in supernova remnants might provide an interesting estimate of the density fluctuations due to interstellar turbulence. A clear test of this picture would be measurement of the ripples at smaller scales. The amplitude divided by the wavelength ought to scale as the square root of the density amplitude, or as the $L^{5/6}$ for Kolmogorov turbulence.

5. SUMMARY

The rippled structure of the non-radiative shock wave in the northern Cygnus Loop appears to result from density fluctuations in the pre-shock medium rather than from instabilities in the shocked gas. The density fluctuations seem consistent with interstellar turbulence. It is possible that the pre-shock gas has been affected by the SN precursor (e.g., Levenson, Graham, & Snowdon 1999), but the amplitude is not unreasonable for the average ISM turbulence.

Overall, it seems possible that one could fit the amplitudes and wavelengths of ripples in non-radiative shocks in order to estimate the density fluctuation amplitudes in the pre-shock gas. This method is sensitive to weak perturbations, as opposed to the high-density contrast clouds that produce the features investigated by Levenson et al. (1999) and Patnaude et al. (2002). In contrast to radio scintillation measurements, it measures the total density, and it pertains to a specific region of space rather than a line-of-sight average. A real assessment of this technique will require a realistic calculation of the propagation of a strong shock through a turbulent medium, including the correlations between density and velocity

REFERENCES

Aschenbach, B., Egger, R., & Trümper, J. 1995, Nature, 373, 587
Bertschinger, E. 1986, ApJ, 304, 154
Blair, W. P., Sankrit, R., Raymond, J. C., & Long, K. S. 1999, AJ, 118, 942

Chevalier, R. A., & Raymond, J. C. 1978, ApJ, 225, L27

Cho, J., Lazarian, A., & Vishniac, E. T. 2002, ApJ, 566, L49

Fesen, R. A., & Itoh, H. 1985, ApJ, 295, 43

Gaetz, T. J., Edgar, R. J., & Chevalier, R. A. 1988, ApJ, 329, 927

Ghavamian, P., Raymond, J., Smith, R. C., & Hartigan, P. 2001, ApJ, 547, 995

Ghavamian, P., Winkler, P. F., Raymond, J. & Long, K. S. 2002, ApJ, 572, 888

Hester, J. J. 1987, ApJ, 314, 187

Hester, J. J., Danielson, G. E., & Raymond, J. C. 1986, ApJ, 303, L17

Hester, J. J., Raymond, J. C., & Blair, W. P. 1994, ApJ, 420, 721

Innes, D. E. 1992, A&A, 256, 660

Innes, D. E., Giddings, J. R., & Falle, S. A. E. G. 1987, MNRAS, 226, 671

Laming, J. M., Raymond, J. C., McLaughlin, B. M., & Blair, W. P. 1996, ApJ, 472, 267

Levenson, N. A., Graham, J. R., Keller, L. D., & Richter, M. 1998, ApJS, 118, 541

Levenson, N. A., Graham, J. R., & Snowden, S. L. 1999, ApJ, 526, 874

Levenson, N. A., Graham, J. R., & Walters, J. L. 2003, RevMexAA(SC), 15, 252 (this volume)

Long, K. S., Blair, W. P., Vancura, O., Bowers, C. W., Davidsen, A. F., & Raymond, J. C. 1992, ApJ, 400, 214

Long, K. S., Reynolds, S. P., Raymond, J. C., Winkler, P. F., Dyer, K. K., & Petre, R. 2003, ApJ, submitted

Minter, A. H., & Spangler, S. R. 1996, ApJ, 458, 194

Patnaude, D. J., Fesen, R. A., Raymond, J., Levenson, N. A., Graham, J., & Wallace, D. J. 2002, AJ, 124, 2118

Raymond, J. C. 1979, ApJS, 39, 1.

Raymond, J. C., Blair, W. P., Fesen, R. A., & Gull, T. R., Jr. 1983, ApJ, 275, 636

Raymond, J. C., Blair, W. P., & Long, K. S. 1995, ApJ, 454, L31

Raymond, J. C., Davis, M., Gull, T. R., & Parker, R. A. R. 1980, ApJ, 238, L21

Raymond, J. C., Ghavamian, P., Sankrit, R., Blair, W. P., & Curiel, S. 2003, ApJ, submitted

Raymond, J. C., Hester, J. J., Blair, W. P., Fesen, R. A., & Gull, T. R. 1988, ApJ, 324, 869

Sankrit, R., & Blair, W. P. 2002, ApJ, 565, 297

Sankrit, R., Blair, W. P., Raymond, J. C., & Long, K. S. 2000, AJ, 120, 1925

Szentgyorgyi, A. H., Raymond, J. C., Hester, J. J., & Curiel, S. 2000, ApJ, 529, 414

Treffers, R. R. 1981, ApJ, 250, 213

Wang, C., & Chevalier, R. A. 2001, ApJ, 549, 1119

Winkler, P. F., & Long, K. S. 1997, ApJ, 491, 829

Vishniac, E. T. 1983, ApJ, 274, 152

Vishniac, E. T., & Ryu, D. 1989, ApJ, 337, 917

John Raymond: Center for Astrophysics, 60 Garden St., Cambridge, MA 02138, USA (jraymond@cfa.harvard.edu).